A comparison of volcanic ash source term characteristics estimated by source inversion and plume rise modelling methods: Raikoke 2019

Journal of Volcanology and Geothermal Research 462 (2025) 108304

Contents lists available at ScienceDirect

Journal of Volcanology and Geothermal Research

journal homepage: www.journals.elsevier.com/journal-of-volcanology-and-geothermal-research

A comparison of volcanic ash source term characteristics estimated by source inversion and plume rise modelling methods: Raikoke 2019

Natalie J. Harvey[a,*], Michael Herzog[b], Helen F. Dacre[a], Helen N. Webster[c,d]

[a] Department of Meteorology, Univeristy of Reading, Reading RG6 6BB, UK
[b] Department of Geography, University of Cambridge, Cambridge CB2 3EN, UK
[c] Met Office, FitzRoy Road, Exeter EX1 3PB, UK
[d] Faculty of Environment, Science and Economy, University of Exeter, Exeter EX4 4QF, UK

ARTICLE INFO

Keywords:
Eruption source parameters
Volcanic plume
Source inversion
Volcanic eruption column modelling

ABSTRACT

Predictions of volcanic ash location and concentration following an eruption rely heavily on estimates of source term characteristics including mass eruption rate, vertical distribution of ash and particle size distribution. These characteristics can be provided by several methods including (i) preset values based on historical data, (ii) near-source plume rise model simulations, (iii) a combination of satellite retrievals and long-range dispersion model simulations (known as source inversion). For the first time, this study presents a comparison of source term characteristics from these different methods. The study focuses on the 2019 Raikoke eruption and analysis of the volcanic ash cloud 150 km downwind from the volcano vent, representing an effective source term for the dispersion of ash in the distal volcanic cloud. Results indicate good agreement in the vertical distribution of ash between the plume rise and source inversion methods but large differences in estimates of the horizontal mass flux at this distance. The plume rise model demonstrates the rapid sedimentation and deposition of coarse ($> 100\mu$m diameter) ash particles close to the volcano vent resulting in a particle size distribution comparable to the preset distribution used operationally by the London VAAC at this range. These results suggest that source inversion can provide a computationally cheaper alternative to the 3D plume rise method for estimating the vertical distribution of ash, and that the assumption of near-source fallout of coarse particles in the preset particle size distribution holds fairly well. Further investigations are recommended including particle aggregation effects to understand differences in estimates of the effective mass eruption rate.

1. Introduction

In the event of a volcanic eruption, the airline industry need to make decisions quickly about which flight routes are safe to operate and ensure airborne aircraft land safely. Safety is key, but re-routing aircraft and blanket cancellations come with a large economic cost.

These high-impact decisions are currently based on information from long-range atmospheric dispersion model simulations which are designed to represent the dispersion of ash in the *distal* volcanic cloud. The term distal is used here to refer to the regime during which interaction of the volcanic cloud with the ambient atmosphere (via process such as entrainment, radiative heating and wind plume bending) and changes to the particle size distribution (due to particle aggregation/disaggregation) are assumed to be small. Thus these simulations rely heavily on estimates of *effective* source term characteristics including mass eruption rate, vertical distribution of ash and particle size distribution. The effective volcanic ash source characteristics contains only the part of the total ash emitted from the volcano vent that undergoes long-range transport. The ash available for long range transport is a particular hazard for aircraft. This effective volcanic ash source term typically contains only fine ash particles. (In some literature it is also referred to as the pseudo-source term). In emergency response situations, choices for the mass eruption rate, vertical distribution of ash and particle size distribution need to be made for dispersion model simulations to be performed.

Empirical relationships, based on historical ash deposits and plume height reports from previous eruptions, can be used to estimate mass eruption rates (e.g., Sparks et al., 1997; Mastin et al., 2009; Aubry et al., 2021). Using these relationships requires information about the height of the ongoing eruption column which can be provided by various

* Corresponding author.
E-mail address: n.j.harvey@reading.ac.uk (N.J. Harvey).

https://doi.org/10.1016/j.jvolgeores.2025.108304
Received 8 October 2024; Received in revised form 19 February 2025; Accepted 21 February 2025
Available online 4 March 2025

sources. In quasi-real time there are several satellite and ground-based remote sensing techniques that can be used to estimate the ash plume height (e.g., Oppenheimer, 1998; Petersen et al., 2012). Additionally if it is an inhabited region, plume height can be estimated by local observers. Most recently estimates of plume height have been made automatically from a calibrated visible camera in real-time (Aravena et al., 2023). However, the preset empirical functions used to predict mass eruption rate from observed plume height do not account for all relevant physical processes that may affect the relationship, such as the impact of the meteorological situation (e.g., wind bent plumes Woodhouse et al., 2013; Dürig et al., 2022, 2023). This, coupled with the reliance on information from historical eruptions, can lead to large uncertainties in mass eruption rate estimates, which in turn impacts the simulated ash location and concentration. For example, Dioguardi et al. (2020) found that a 6 km plume with a $\pm$ 1 km uncertainty can lead to the geographical area affected by ash with concentrations exceeding 2 mg m^{-3} changing by a factor of three. Furthermore, estimates of the effective mass eruption rate, required for long-range modelling of the distal ash cloud, require knowledge of the fraction of the total eruptive mass contained in the fine ash component (known as the distal fine ash fraction, Dacre et al. (2011)). For current, operational modelling a preset distal fine ash fraction (DFAF) of 5% is typically assumed based on analysis of past eruptions (Webster et al., 2012; Devenish et al., 2012; Dacre et al., 2013).

Developments in satellite retrieval techniques have enabled estimates of ash column loading, ash cloud top height and ash effective radius (e.g., Francis et al., 2012; Pavolonis et al., 2013; Grainger et al., 2013; Prata et al., 2022; Guerrieri et al., 2023). A number of studies have shown that it is also possible to estimate mass eruption rates but these rely on a number of assumptions (e.g., Woods and Kienle, 1994; Pouget et al., 2013; Prata et al., 2021) and are not routinely applicable in real-time. A more advanced technique to calculate mass eruption rate than using a preset empirical function and DFAF, and which exploits advances in satellite retrieval techniques, is known as source inversion modelling. Inversion modelling combines retrievals of ash column loading with simulations from a volcanic ash transport and dispersion model (VATDM). Since satellites cannot typically detect particles greater than 30 μm diameter, the source inversion method provides an estimate of the effective mass eruption rate. There are many published approaches that use inversion modelling to estimate both effective mass eruption rates and vertical ash distributions for volcanic eruptions (e.g., Kristiansen et al., 2012; Schmehl et al., 2012; Denlinger et al., 2012; Pelley et al., 2021; Zidikheri et al., 2017a, 2017b; Harvey et al., 2020, 2022). This effective source term estimate can have vertical information and be time varying, or even an ensemble of estimates.

A third method to determine source term characteristics is to run a plume rise model. Plume rise models are designed to represent the dispersion of ash in the near-source regime. As such, they contain both fine ash and coarse ash particles representing the *total* eruption source term. Plume rise models represent the dynamical evolution of the eruption column as it interacts with the surrounding environment. 1D (and some 0D) plume rise models use simplifying assumptions and hence depend on the estimation of certain parameters (e.g., Bursik, 2001; Mastin, 2007; Degruyter and Bonadonna, 2012; Woodhouse et al., 2013; Girard et al., 2014; Folch et al., 2016; Cerminara, 2015; de Michieli Vitturi et al., 2015). Crucially, the entrainment of air into the volcanic plume is based on two coefficients: One due to the crosswind field and the other due to the turbulence in the rising buoyant jet. Varying these entrainment parameters can lead to large differences in the solutions found but they are difficult to estimate as the required observations to determine them are not available. In 1D models the feedback from plume to atmosphere is usually ignored. 3D plume rise models are based on first principles and have a relatively small number of parameterized coefficients compared to lower order models (e.g., Oberhuber et al., 1998; Neri et al., 2003; Suzuki et al., 2005; Suzuki and Koyaguchi, 2009; Cerminara et al., 2016; Carazzo and Jellinek, 2013; Cao et al., 2018). A comparison between 1D and 3D plume rise models presented in Costa et al. (2016) found that 1D formulations are sufficient to represent the processes in a weak volcanic plume but they could not capture complex features, such as large vortices and partial column collapse, which are often present in strong volcanic plumes. Analysis performed in Suzuki et al. (2016) suggests the differences between distinct 3D model formulations and numerics are enhanced in strong plumes due to unstable flow dynamics. However, due to the complexity of the equation sets, 3D plume rise models are computationally very expensive so simulations are restricted to small domains (typically 0–10 km) and short simulation lengths so they are only suitable for proximal (near-vent) predictions and cannot be used to simulate long-range transport of volcanic ash.

The coupling of a near-source 1D plume rise model to a long-range atmospheric dispersion model was investigated in Bruckert et al. (2021) and Plu et al. (2021), where FPLUME Folch et al. (2016) was coupled to full atmospheric modelling systems ICON-ART (ICOsahedral Nonhydrosatic - Aerosols and Reactive Trace gases) and MOCAGE (MOdele de Chimie Atmospherique de Grande Echelle), respectively. In both cases, the combination gave a more accurate representation of the source term characteristics and thus a significantly improved ash forecast. Cao et al. (2021) also found that removing assumptions about the plume geometry by coupling the Plume-SPH (Smoothed Particle Hydrodynamics) plume rise model to the PUFF VATD model improved the skill of simulations of the 1991 eruption of Pinutubo. They suggest that this type of coupling provides a path to better forecasts lessening the need for user intervention, or attempts to observe details of an eruption that are beyond the resolution of any potential satellite or ground-based technique. A similar approach has been taken in predicting tephra fall out by Tadini et al. (2020). However, coupling with a 3D plume rise model, as in Cao et al. (2021), is too computationally expensive to run in an emergency response situation as it takes tens of minutes for plumes to reach a steady height. Coupling with a 1D plume rise model (as in Plu et al. (2021); Bruckert et al. (2021)) removes the needed to apply a preset distal fine ash fraction to standalone dispersion simulations, but replaces it with the need to estimate parameters representing the entrainment of air into the rising buoyant volcanic plume. Despite this progress in coupling plume rise and atmospheric dispersion models there is no literature comparing source inversion and 3D plume rise model estimates of volcanic source characteristics or the volcanic ash distributions they simulate. This is likely due to the differing spatial and temporal scales that these different models are applied to and their applications. VATDMs are used to produce ash cloud forecasts for the duration of an eruption (which could continue for a number of weeks) during which the ash cloud could span a very large area. Conversely, plume rise models seek to fully represent the dynamical and thermodynamic processes within the rising plume itself thus typically, for computational reasons, focus on the region closest to the volcano vent.

The residence time of ash injected into the atmosphere is governed by the size, shape and density of the ash particles (e.g., Beckett et al., 2015; Osman et al., 2020) and the injection height which impacts the deposition due to sedimentation of the ash particles, in addition to removal by wet and dry deposition processes. Therefore another important source term characteristic that needs to be specified to create a long-range volcanic ash forecast is the particle size distribution (PSD). However, this information is difficult to determine and is certainly not available in real time so preset PSDs are typically used operationally (e.g. Beckett et al., 2020). To represent the effective PSD it is commonly assumed that particles with diameters greater than 100 μm are removed from the atmosphere near the vent and are not available for long range transport Beckett et al. (2020). Thus effective PSDs used in VATD models only contain fine ash particles. However, there is evidence from in-situ measurements that the PSD can evolve overtime especially for long eruptions (e.g., Dacre et al., 2013) and that large ash particles ($>$ 100 μm) can travel long distances from the volcano vent (Watson et al., 2016; Saxby et al., 2020). A possible mechanism for the large distances travelled by these particles is rafting (Rossi et al., 2021), which is not currently represented in VATDMs. To the authors knowledge a comparison of the evolving total PSD in plume-rise models and the preset effective PSD used in long-range dispersion models has not been attempted before.

In this study an estimate of the effective source term for the 2019 eruption of the Russian volcano Raikoke is determined using a source inversion model, Inversion Technique for Emissions Modelling (InTEM) (Pelley et al., 2021), developed by the UK Met Office. This effective source term is used as input to the Numerical Atmosphere Modelling-dispersion Environment (NAME) (Jones et al., 2007) to simulate volcanic ash dispersion. This volcanic ash distribution is compared to a simulation performed using the plume rise model Active Tracer High Resolution Atmospheric Model (ATHAM) (Grant et al., 2012; Herzog et al., 2003). The choice to use the state-of-the-art ATHAM rather than a computationally cheaper 1D plume rise model is to enable a comparison of the horizontal distribution of the plume and to avoid introducing further uncertainties related to assumptions about the source vent size and entrainment that are necessary when using a 1D model. The analysis here focuses on 2 main questions:

1. How does the ash distribution in a NAME-InTEM simulation compare to that simulated by ATHAM in terms of magnitude and vertical distribution?
2. At what range (if any) is the preset effective particle size distribution used in NAME consistent with the time-evolving total particle size distribution from ATHAM?

To address these questions many choices need to be made when performing the ATHAM and NAME-InTEM simulations. Given the lack of observational constraints here we have made choices that are consistent with previous case studies using ATHAM and the operational use of NAME at the London Volcanic Ash Advisory Centre, although it is noted that it is possible that many other plausible choices could be used.

Section 2.1 describes the details of the 2019 Raikoke eruption. The tools and data used in this study are described in Sections 2.2–2.4. The main results of this work are presented in Section 3. Finally, a summary, conclusions and implications for future work are presented in Section 4.

2. Case study description and tools

The research questions outlined in Section 1 will be addressed using the 2019 Raikoke eruption as a case study.

2.1. Case study: Raikoke 2019

Raikoke is an uninhabited volcanic island in the northwest Pacific Ocean (48.2°N, 153.3°E). Its most recent explosive eruption started at approximately 18:00 UTC on 21 June 2019 after which 10 explosive events were identified (see Table 1 in Bruckert et al., 2021). Nine of these events were short lived (less than 25 min), however emissions were more or less continuous between 22:40 UTC 21 June to 01:55 UTC 22 June. This period is referred to as phase 7 in Bruckert et al. (2021). Due to the computational expense of running the ATHAM simulation, it is this quasi-steady phase that will be considered in this study. At this time it was estimated that the eruptive plume height was 13.75 km above sea level (asl) (Bruckert et al., 2021; Global Volcanism Program, 2019) and visible satellite imagery suggests the formation of an umbrella cloud. There is evidence from GOES-R near limb imagery that parts of the plume may have reached up to 16.5 km asl (Horváth et al., 2021). It is estimated that this eruption injected approximately 1.5 Tg of sulphur dioxide into the stratosphere, which is the largest such emission since the 2011 Nabro eruption.

Table 1
The particle size distributions (PSD) used in ATHAM and NAME in this study. ATHAM uses the total PSD whereas NAME uses an effective PSD. The effective PSD only includes fine ash emissions that are available to be transported long distances from the volcano vent. Note that the mass fraction for NAME is the fraction of mass from 0.1 to 100 μm, whereas the mass fraction for ATHAM is the fraction of mass from 1 to 30,000 μm.

Particle diameter (μm)	Mass fraction	
	ATHAM	NAME
0.1–0.3	0	0.001
0.3–1.0	0	0.005
1.0–3.0	0.008	0.05
3.0–10.0	0.023	0.2
10.0–30.0	0.067	0.7
30.0–100	0.181	0.044
100–300	0.193	0
300–1000	0.229	0
1000–3000	0.178	0
3000–10,000	0.092	0
10,000–30,000	0.020	0

2.2. InTEM for volcanic ash

The Inversion Technique for Emissions Modelling (InTEM) for volcanic ash is a Bayesian inversion system for estimating effective volcanic ash emissions using satellite retrievals of ash column loading, VATDM simulation output and a prior estimate of the effective emission (Pelley et al., 2021). Using these input data, it provides a best estimate of the effective emissions profile for fine ash that can undergo long range dispersion. This posterior effective emission profile can either be determined using satellite retrievals of ash only or of both ash and pixels free of ash and meteorological cloud. The typical source resolution used in InTEM is a time resolution of 3 h and a vertical resolution of 4 km, however in this study the resolution has been increased to be hourly and 1 km in the vertical to match more closely to the plume model simulation.

InTEM has recently been used to assess the impact of ensemble meteorology on estimates of effective volcanic ash emissions from the 2011 Grímsvötn (Harvey et al., 2020) and Raikoke eruptions (Harvey et al., 2022). Webster and Thomson (2022) use two measures output from the InTEM Bayesian framework, to determine a “best” meteorological data set from within an ensemble of numerical weather prediction forecasts for the 2011 Grímsvötn eruption. They show that using this best meteorological dataset leads to more accurate ash forecasts.

2.2.1. Estimate of the prior effective source term

The prior estimate of the effective emissions is informed by an estimate of the plume height and its evolution during the eruption. (Note in the rest of this paper, plume height refers to the maximum height that the ash reaches above the volcano vent.) It is assumed that there is an error on the plume height of ±2 km and that the vertical distribution of ash of the prior mean is uniform. These are the default assumptions applied when using InTEM and have been used in other studies using InTEM (e.g., Webster and Thomson, 2022). The plume height error of ±2 km is based on the estimate of rise height error assumed for the Eyjafjallajökull 2010 (Arason et al., 2011) and Grímsvötn 2011 eruptions. This value is broadly consistent with the size of the discrete steps in the estimated rise height time series for those eruptions (see Pelley et al. (2021)). Using a prior mean profile with non-zero effective emissions at all possible heights and with large uncertainties enables significant adjustments away from the prior mean. This means the posterior effective emissions can have very different vertical distributions and magnitudes compared to the prior mean. The empirical relationship in Mastin et al. (2009) and a DFAF of 5 % is used to determine the prior effective mass eruption rate. The use of a prior ensures that the posterior estimate is based on information known about the eruption and is not overfit to the satellite retrievals. Full details of the determination of the prior estimate can be found in Thomson et al. (2017). In this study the prior effective source term is based on a plume height of 18 ± 2 km avl, which is higher than the information provided by the Tokyo VAAC and Bruckert et al. (2021) but consistent with other remote sensing estimates (e.g., Horváth et al., 2021).

2.3. Satellite retrievals

The satellite retrievals used in this study are from the geostationary Himawari-8 satellite. This instrument came into operation in July 2015 and has 16 spectral channels (Bessho et al., 2016). It is ideally suited to provide observations following an eruption as it has high temporal (10 min) and spatial (2 km at nadir for the infrared bands) resolution.

The retrieval algorithm used here is based on the method described in Francis et al. (2012) and uses a reverse absorption technique with slight adaptations for the channels of the Advanced Himawari Imager and has been optimised for the 2019 Raikoke eruption. To reduce false detections over arid land surfaces and at a high satellite zenith angle, several geographical filters are used. Checking the consistency of ash detection in neighbouring pixels also removes other false detections. The detection limit for thermal infrared column load retrievals is 0.2 g m^{-2} (Prata and Prata, 2012).

Where ash is detected, the retrieval algorithm determines the ash column loading. These pixels are flagged as containing ash. If a pixel is free from both ash and meteorological cloud, then it is flagged as a clear-sky pixel. Pixels that do not have detectable ash and are not flagged as clear skies are unclassified (e.g., they may contain meteorological cloud). The retrieved column loadings are further processed onto the NAME output grid (approximately 40 km × 40 km in mid-latitudes) and averaged over 1 h. Here, as in the default setup of InTEM, to be used in the InTEM inversion 50 % or more satellite pixels in a grid box must contain ash or more than 90 % of pixels must be classified as ash or clear skies. A grid box is deemed to be a clear sky observation if all classified pixels within a grid box are flagged as clear sky pixels. A grid box is considered to be an ash grid observation if any pixels are classified as ash, with the column loading in this grid box given by the mean of all the classified pixels (including clear skies).

2.3.1. VATDM simulations

The VATDM simulations in this study are performed using the Numerical Atmospheric-dispersion Modelling Environment (NAME) (Jones et al., 2007). NAME includes parameterisations of sedimentation and turbulent dry deposition (Webster and Thomson, 2011), wet deposition (Webster et al., 2017) as well as advection by the ambient winds and dispersion due to turbulent motions (Webster et al., 2018). It is assumed here that the ash particles have a density of 2300 kg m^{-3} and are spherical (Bonadonna and Phillips, 2003).The choice of spherical particles is justified as Saxby et al. (2018) found that forecasts of distal ash concentration using particle size distributions of 0.1–100 μm and 0.1–250 μm show relatively good agreement between a spherical and non-spherical case for the first 36 h after an eruption. In the case of Raikoke 2019, there are very few direct observations of the fine ash properties (e.g. density and PSD) in the literature. Therefore, the typical values used for density and shape in InTEM are assumed. Although it is noted that in an emergency response situation it may be preferable to produce ensemble forecasts which explicitly represent the uncertainties related to these choices. To enable a fair comparison with satellite imagery the predicted NAME ash cloud is restricted to including only particles between 1 and 30 μm diameter. This is because satellite retrievals cannot typically detect particles larger that this. In reality, there is likely to be ash with larger diameters present following an eruption, especially close to the vent as fine ash is only a fraction of the total ash emissions from the volcano. Therefore, it is important to note the range of particle sizes emission estimates represent and that the total ash emission may differ from this. Additionally, remote sensing techniques have a maximum detection limit (Saint et al., 2024) which can impact retrieval uncertainty. Other inversion systems developed for this application (e.g., Stohl et al., 2011) make an assumption about the PSD consistent with the one made in InTEM. The particle size distribution used in the VATDM simulations performed in this study is shown in Table 1. This PSD is chosen as it is the one of the options for PSD used by the London VAAC in an emergency response situation when no case specific information is available in real time (Beckett et al., 2020).

The NAME simulations have nominal source term components with 1 km vertical resolution for each hour and with a release rate of 1 g s^{-1}. Predictions of ash column loads for an arbitrary effective source term can then be easily determined using a linear combination from each possible nominal source term component. Note that the version of NAME used here does not include a parameterisation for aggregation of ash particles or any representation of processes driven by the eruption dynamics (e.g., Woodhouse et al., 2013). InTEM determines an effective source term accounting for these missing processes.

All NAME simulations conducted in this study are driven using the UK Met Office analysis data from the global version of the UK Met Office's NWP model, the Unified Model Walters et al. (2017) which has a horizontal resolution of approximately 10 km. The simulations conducted here update the meteorological data every 3 h. The NAME output grid used here has a horizontal resolution of 0.5625 × 0.375 degrees (approximately 40 km × 40 km in mid-latitudes). This is sufficient to show the structure of the long-range ash cloud.

2.3.2. The inversion algorithm

Within the InTEM inversion algorithm, the satellite retrievals, NAME simulations and prior effective source term estimate are combined to give a posterior distribution of the effective source term. Within InTEM, the peak of this Gaussian distribution, with a non-negative emissions constraint applied, is taken as the best estimate of effective emissions. The Lawson and Hanson non-negative least squares algorithm Lawson and Hanson (1974, 1995) is used to minimise a quadratic cost function, representing the simultaneous fit of the VATDM simulations and satellite retrievals, and between the emission estimate and the prior. This algorithm uses an active set approach, iteratively refining the solution by adjusting the variables allowed to be non-zero and efficiently solving constrained subproblems using Cholesky factorization. It is suitable as it quickly converges in a finite number of iterations. Therefore the speed of the InTEM system is limited by the length of time it takes to perform the NAME simulations. The InTEM derived best estimate of the effective mass eruption rate as a function of height and time can then be used as the ash emission profile in simulations used to forecast the evolution of the volcanic ash cloud. For a full description of the inversion scheme see Pelley et al. (2021) and Thomson et al. (2017).

2.4. ATHAM

ATHAM is a non-hydrostatic atmospheric circulation model focussing on cloud resolving scales of tens of meters to tens of kilometers (Oberhuber et al., 1998; Herzog et al., 2003). It has been used to simulate volcanic plumes forced at the surface boundary by parameters describing the eruption such as vent size, exit velocity and temperature, along with composition of the plume mixture. The dynamical core of the model solves the compressible Euler equations. To avoid a very large equation set (as each ash size needs its own set of equations), it is assumed that the mixture of gaseous and particulate components are in dynamical and thermal equilibrium (Oberhuber et al., 1998; Herzog et al., 2003). This means that there is instantaneous exchange of heat and momentum in the horizontal. Momentum exchange is also instantaneous in the vertical, i.e. particles are assumed to move with their terminal fall velocity relative to the gas. These assumptions are valid provided the particles are small and that the time step is large compared to the time required to reach equilibrium. The partial differential equations are solved using a finite difference method. The transport equations are formulated in flux form to conserve both mass and momentum. Over- and under-shoots in the advection scheme are avoided by using a correction term as in Smolarkiewicz (1984). Time integration follows a generalised Crank-Nicholson scheme (Crank and Nicolson, 1947). The sub-grid turbulent mixing is based on an anisotropic turbulent kinetic energy scheme differentiating between horizontal and vertical directions (described in Herzog et al. (2003)) and phase changes associated with cloud micro-physics are also included (Herzog et al., 1998).

A non-uniform stretched grid is used in both the horizontal and the vertical. This enables a higher resolution at the centre of model domain with the highest resolution around the volcano vent (approximately 18 m $\times$ 18 m $\times$ 18 m). In this study the grid is 416 $\times$ 288 $\times$ 181 points in the x, y and z directions respectively with a domain size of 330 km $\times$ 160 km $\times$ 30 km. At the downwind boundary, the horizontal resolution is reduced to approximately 2 km $\times$ 2 km. The vertical grid is fixed but with higher resolution near the surface (18 m) stretching to approximately 250 m at 10 km and 662 m at the lid. The use of variable resolution enables the simulation of processes that occur at the microscale at the vent and mesoscale downwind. Note that this is a much finer grid than what is used here (and operationally) in the NAME simulations. The top boundary is a rigid lid with a free slip boundary condition. At the bottom boundary, surface drag is implemented using Monin Obukov similarity theory with the assumption of neutral stratification. At the lateral boundaries, a Neumann boundary condition is imposed. The simulations are initialised with vertical profiles of temperature, humidity and wind speed taken from meteorological analysis. In the simulation presented here profiles were taken from ERA5 reanalysis (Hersbach et al., 2020) at 23:00 UTC 21 June 2019.

Due to the computational expense of running the ATHAM simulation it is only possible to run one simulation in this study with one choice of model parameters. The input parameters and ash particle size distribution chosen can be found in Tables 1 and 2, respectively. The total mass eruption rate for phase 7 of the eruption is taken from Bruckert et al. (2021) and is based on the empirical relationship of Mastin et al. (2009). The use of the Mastin et al. (2009) relationship is justified as satellite images suggest that the plume penetrates into the stratosphere and spreads out radially. The winds in the stratosphere are between 5 and 10 m/s (Fig. 1(d)), which is unlikely to result in plume bending according to Woodhouse et al. (2013) (Fig. 2). Also, other studies (e.g. Harvey et al., 2022) have found that the Mastin et al. (2009) relationship over estimates the mass eruption rate for the Raikoke eruption when compared to satellite estimates. If the plume was significantly bent over the Mastin et al. (2009) relationship would underestimate the mass eruption rate.

In the ATHAM simulation 9.8% of the total emitted mass is transported by fine ash particles (diameters $< 30\ \mu$m, Table 1).The PSD used in the ATHAM simulation is based on the one for Grimsvotn 2011 in Höskuldsson et al. (2018). This has then been converted from phi classes and mapped on to the default NAME bins (shown in Table 1) using a piece constant distribution. The maximum ash radius used in ATHAM is 1.5 cm. This mapping was used to ensure that the PSDs used in the two sets of simulations are as close as possible with respect to fine ash.

Table 2
Input parameters used in the ATHAM simulation presented in this study.

Parameter	Value
Vent elevation (m)	551
Eruption duration (minutes)	195 (120 min of simulation)
Mass eruption rate (kg/s)	6.4×10^6
Exit velocity (m/s)	105
Exit temperature (K)	1273
Exit water fraction (%)	3
Ash density (kg/m^3).	1600–2600 (Bonadonna and Folch (2011))

3. Results

This section presents the evolution of the ash cloud in the ATHAM simulation and the NAME-InTEM simulations for phase 7 of the 2019 Raikoke eruption (Bruckert et al., 2021). The vertical ash distribution 150 km from the volcano vent from these simulations are compared, representing an effective source term for the dispersion of ash in the distal volcanic cloud. Finally the evolution of the PSD in the ATHAM simulation is compared to the preset effective volcanic ash PSD used in NAME.

3.1. Evolution of the volcanic plume in the ATHAM simulation

Fig. 1 shows a snapshot of the volcanic plume 120 min into the ATHAM simulation of phase 7 of the Raikoke eruption. By this time the plume has been advected 220 km downwind from the vent (Fig. 1a). The ash at approximately 12 km altitude has travelled the furthest (Fig. 1c). This is the same level as the peak wind speeds prescribed (Fig. 1d). The plume has spread in the cross-plume direction by approximately 60 km and has a maximum height of 18 km avl (Fig. 1b). Peak ash mixing ratios are above the volcano vent and there is evidence of larger ash particles sedimenting out of the ash plume out to 100 km from the vent in the along wind direction (Fig. 1c). Although computational limitations prevent longer simulations using ATHAM (the simulation analysed here took over three weeks to complete on local compute nodes), visual inspection of the ash cloud vertical distribution after 120 min suggests that these heavier particles would be unlikely to travel 150 km downwind from the volcano vent before they are deposited to the surface. There is a small amount of ash that travels in the opposite direction near the the surface. This is due to the wind direction reversing in the atmospheric boundary layer (Fig. 1e).

3.2. InTEM effective source emissions

Fig. 2 shows the prior mean (a) and optimal posterior height-time effective emission rates obtained using ash only satellite retrievals (b) and using ash and clear sky satellite retrievals (c) by InTEM for phase 7 of the Raikoke eruption (21–22 June 2019). For both posterior estimates Himawari retrievals from 21 to 24 June are used. The effective emission profile obtained using the ash only retrievals (Fig. 2) extends up to 20 km above vent level (avl) (as prescribed by the prior) and has significant emissions in the lowest 1 km above the volcano vent. Time-integrated ash emitted in this effective emission profile (TE$_0$, Eq. (1)) is 1.409 Tg, which is a reduction of 12.125 Tg from the prior mean estimate. The effective emissions determined using both clear sky and ash retrievals has a plume height of 17 km avl which is a reduction from the prior and more consistent with the plume height reported by Global Volcanism Program (2019) and determined in Harvey et al. (2022). The reduction in plume height to 17 km is likely due to the significant wind shear in the stratosphere which results in ash being transported in a different direction to the ash lower down in the atmosphere. Therefore it is not possible for ash to be emitted above 17 km and to match the satellite retrieval which includes clear-sky information. The estimated effective emissions immediately above the volcano vent and up to 4 km avl are greatly reduced from both the prior mean and the effective emissions determined just using ash retrievals. The time-integrated estimated effective emissions, TE$_0$, are reduced by a further 70% to 0.433 Tg due to the addition of the information from the clear sky retrievals. This reduction is consistent with Harvey et al. (2022) who applied the same inversion methodology to the whole of the Raikoke 2019 eruption not just phase 7. A previous study using InTEM also found that the choice of satellite information (ash only or ash and clear skies) used can introduce a factor of between 3 and 10 uncertainty in the overall emissions depending on the eruption (Pelley et al., 2021). Therefore, the difference in the inversion estimates is comparable to other sources of uncertainty. The 0.433 Tg estimate is also consistent with the maximum mass found

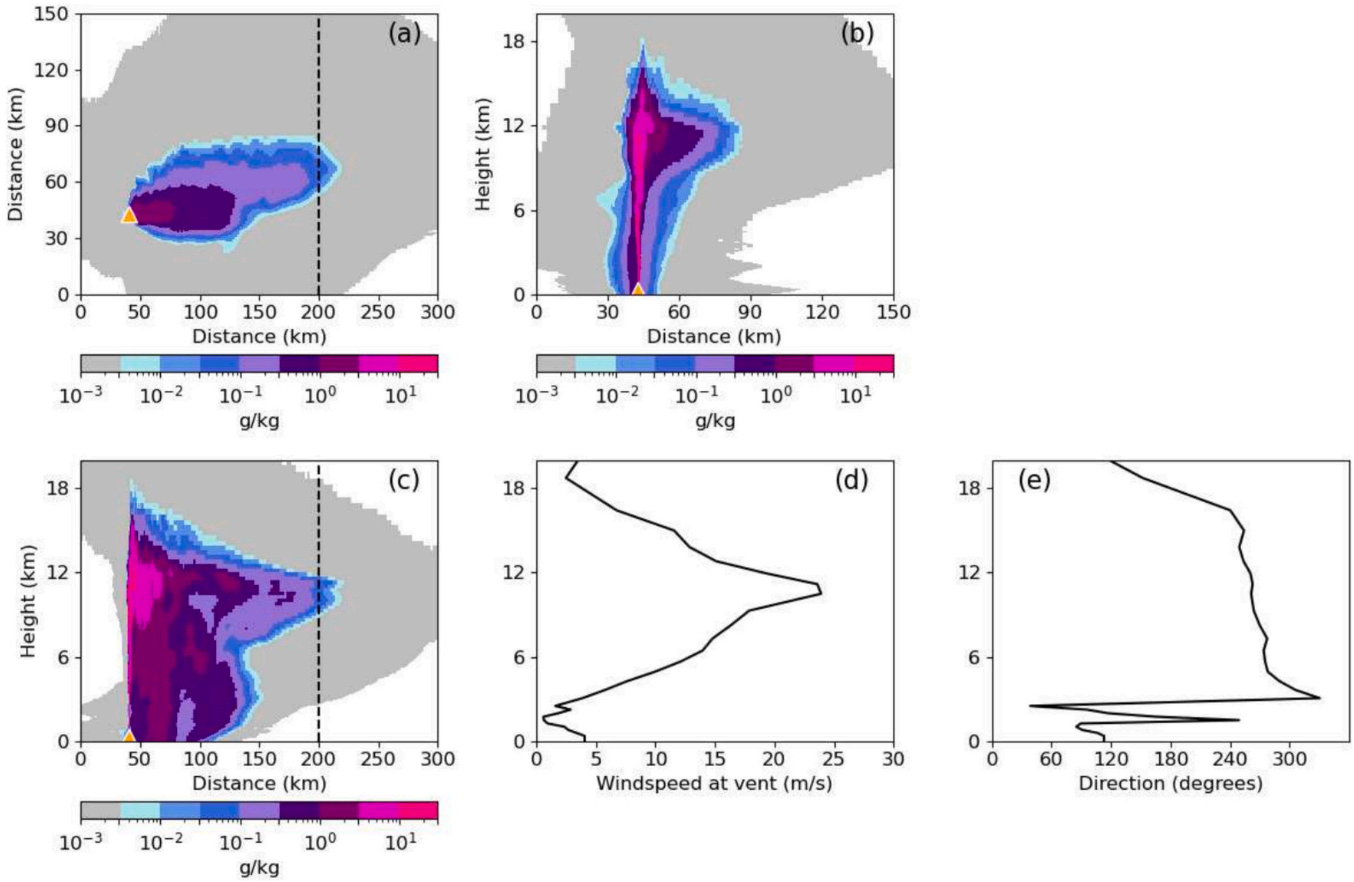

Fig. 1. (a) Plan view of the vertically averaged ash plume (x-axis is distance to the East and the y-axis is the distance to the north) (b) Mean North-South cross section through the ash plume (c) Mean East-West cross section through the ash plume, both at the volcano vent location at 120 min into the ATHAM simulation of phase 7 of the Raikoke eruption. (d) Vertical profile of wind speed and (e) vertical profile of wind direction prescribed in the simulation. Note that the heights here are asl and the dashed black line in panels (a) and (c) indicates 150 km downwind from the volcano vent.

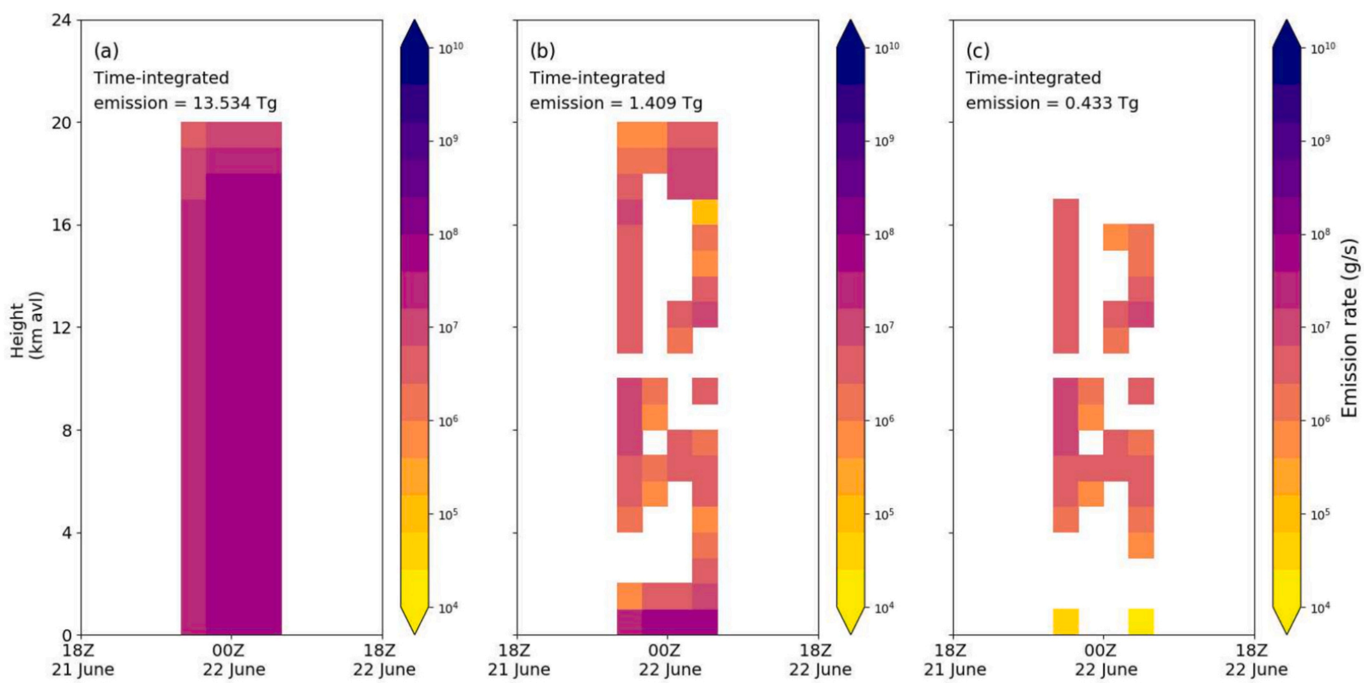

Fig. 2. (a) Prior mean effective emission profile with a uniform vertical ash distribution, (b) optimal posterior time-height effective emission profile determined by InTEM using ash only satellite retrievals (c) optimal posterior time-height effective emission profile determined by InTEM using ash and clear sky satellite retrievals, for phase 7 of the Raikoke eruption. Note the log scale used for the release rate.

in the satellite retrievals scenes used as input to InTEM (0.5 Tg) and estimates of 0.73 ± 0.4 Tg, 0.4–1.8 Tg and 0.49 Tg in Prata et al. (2022), Muser et al. (2020) and Capponi et al. (2021), respectively.

3.3. Comparison of the ash cloud 150 km downwind from the volcano vent

Fig. 3 compares the vertical distribution of ash concentration in a NAME-InTEM simulation to the ash concentration in the ATHAM simulation 150 km from the volcano vent in both simulations and 120 min into the ATHAM simulation and 140 min into the NAME-InTEM simulation (this is 120 min of ash travel time). To make it easier to compare the vertical distributions of fine ash, the ATHAM ash concentrations are re-scaled. To re-scale we calculate the respective time-integrated fine ash emissions, TE_0. Where TE_0 is defined in Eq. (1), E_0 is the mass eruption rate and dt is the duration of phase 7 of the eruption. The ATHAM fine ash concentrations are re-scaled so that the time-integrated fine-ash emission, TE_0, in ATHAM matches the time-integrated emission in the NAME-InTEM simulation (i.e. 0.433 Tg, Fig. 2c).

$$\text{Time-integrated fine ash emission}, TE_0(g) = \int E_0 dt \qquad (1)$$

The scaling factor applied to the ATHAM simulations is 1/10 (i.e. the ATHAM simulation fine ash TE_0 is 10 times larger than that in the NAME-InTEM simulations). This difference in the fine ash mass does not evolve significantly from the vent to 150 km. Note that if the estimate of time-integrated fine ash determined from InTEM using ash-only pixels was considered for comparison with ATHAM, the scaling factor required to match ATHAM and NAME-Intem emissions would change from 0.1 to 0.3, a smaller but still significant discrepancy.

Fig. 3 shows a vertical cross-section through the plume at 155.9^o E in the scaled-ATHAM and NAME-InTEM simulations respectively. Fig. 3(a) shows the scaled-ATHAM concentrations with all ash sizes included whereas Fig. 3(b) shows scaled-ATHAM concentrations for just the fine ash. These figures are very similar, which is expected as 150 km from the volcano vent much of the larger ash has been deposited to the surface whereas the fine ash remains in the ash cloud. Although the simulations have a very different native grid, the structure of the maximum ash concentrations in the NAME-InTEM simulation (Fig. 3(c)) is in a very similar location and of a similar magnitude to the scaled-ATHAM values, at 48.5^o N and at 10 km altitude. Thus, the near-source processes represented in ATHAM do not result in a significantly different vertical distribution when compared to the NAME-InTEM the ash cloud. The plume also has a very similar vertical extent which is shown in Fig. 3(d), although the scaled-ATHAM plume is more peaked.

Fig. 4 shows a comparison of the plan view of the maximum concentration of ash in the ash cloud in the scaled-ATHAM simulation (Fig. 4a and b) and NAME-InTEM simulation (Fig. 4c) at the same time as in Fig. 3. Qualitatively, the fine ash only part of the scaled-ATHAM ash plume has a similar structure to the NAME plume which extends further in both horizontal directions and has similar peak ash concentrations. The difference in the location of the peak ash concentration may be due to the small differences in the 3D winds used in each simulation (ERA5 reanalysis in ATHAM and Met Office Global analysis in InTEM/NAME). Small differences in wind speed and wind direction can lead to significant differences in ash plume structure. In both simulations the concentration of fine ash remains fairly constant in the along-plume direction suggesting little loss of fine ash mass due to sedimentation.

3.4. Comparison of the particle size distributions 150 km downwind from the volcano vent

Fig. 5 shows the ATHAM total PSD at the volcano vent (shown in navy and in Table 1), the effective PSD used in NAME and ATHAM total PSD 150 km downwind from the volcano vent. The initial ATHAM total PSD is quasi-uniform for particles 30–3000 μm in diameter with much smaller mass fractions assigned to particles outside this range. The ATHAM total PSD found at 150 km downwind is more peaked with almost 60% of the mass in the 30–100 μm bin. This is consistent with the assumption that as the distance downwind of the volcano vent increases, the total PSD is restricted by the larger particles (> 30 μm) falling out.

The effective NAME effective PSD is also shown in Fig. 5. At 150 km downwind from the volcano vent, the ATHAM total PSD results in a more similar PSD to that used in NAME. The NAME effective PSD 150 km downwind is almost identical to the preset effective PSD at the volcano vent since deposition of the fine ash particles to the surface is

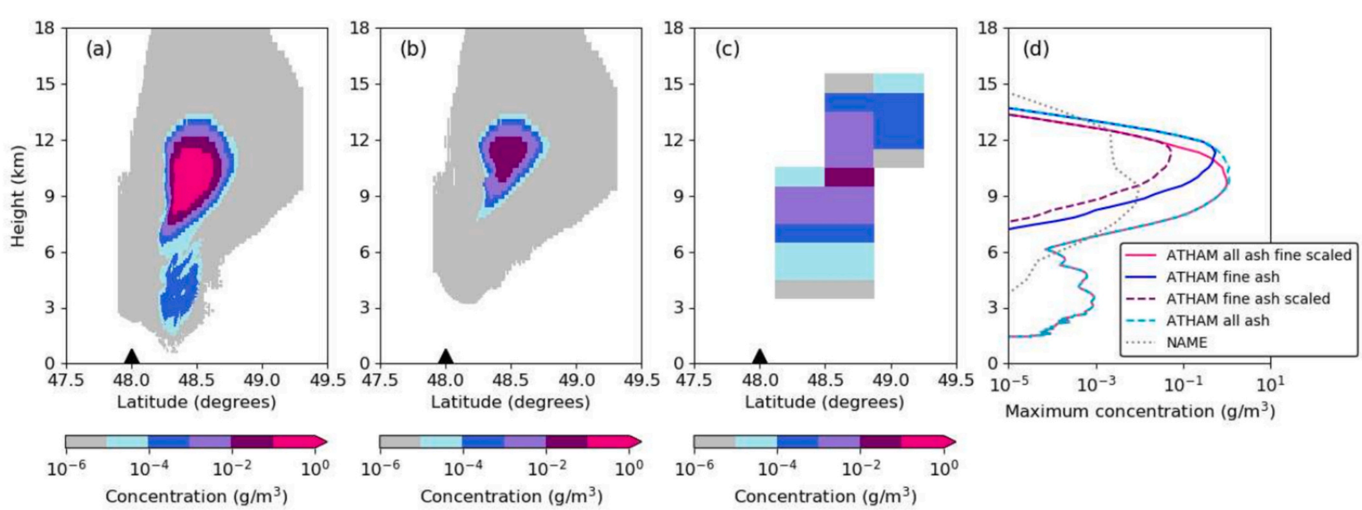

Fig. 3. Vertical cross section of ash concentration through the ash cloud 150 km downwind from the volcano vent at 155.9°E in (a) ATHAM (all ash with fine ash particle sizes scaled so that the time-integrated fine ash mass emitted, TE_0, matches the time-integrated mass emitted in InTEM), (b) ATHAM (fine ash only, scaled so that the TE_0 matches the time-integrated mass emitted in InTEM) and (c) NAME-InTEM simulation using the effective source determined using InTEM (Fig. 2c). (d) shows the vertical profile of the maximum concentration for the NAME-InTEM simulation (grey dotted), scaled-ATHAM simulation (fine ash only as in (b), purple dashed line) and unscaled-ATHAM simulation (fine ash only, blue line), scaled-ATHAM simulation (all ash with fine ash scaled as in (a), pink line) and unscaled-ATHAM simulation (all ash, cyan dashed). Note the logarithmic scale on the x-axis. (For interpretation of the references to colour in this figure legend, the reader is referred to the web version of this article.)

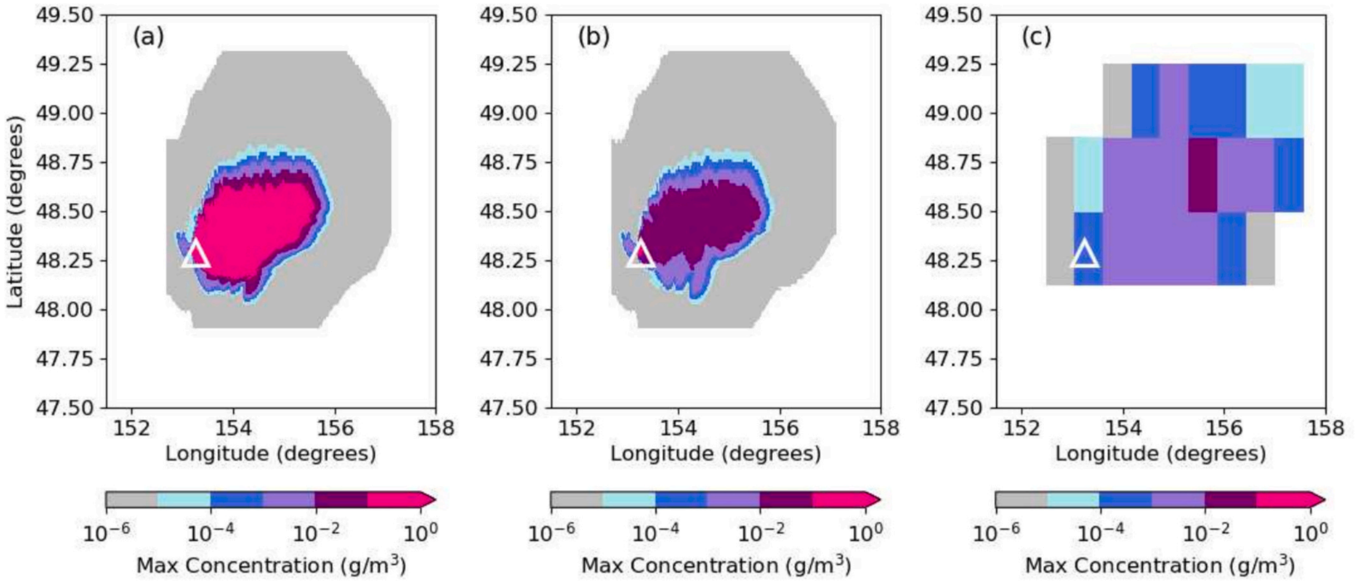

Fig. 4. Plan view of maximum ash concentration in (a) ATHAM simulation (fine ash particles scaled so that the time-integrated fine ash mass matches the time-integrated mass in InTEM as in Fig. 3(a)), (b) ATHAM simulation (fine ash only, scaled so that the time-integrated fine ash mass matches the time-integrated mass in InTEM as in Fig. 3(b)) and (c) NAME-InTEM simulation using the effective source determined using InTEM (Fig. 2c) and at the same time as Fig. 3.

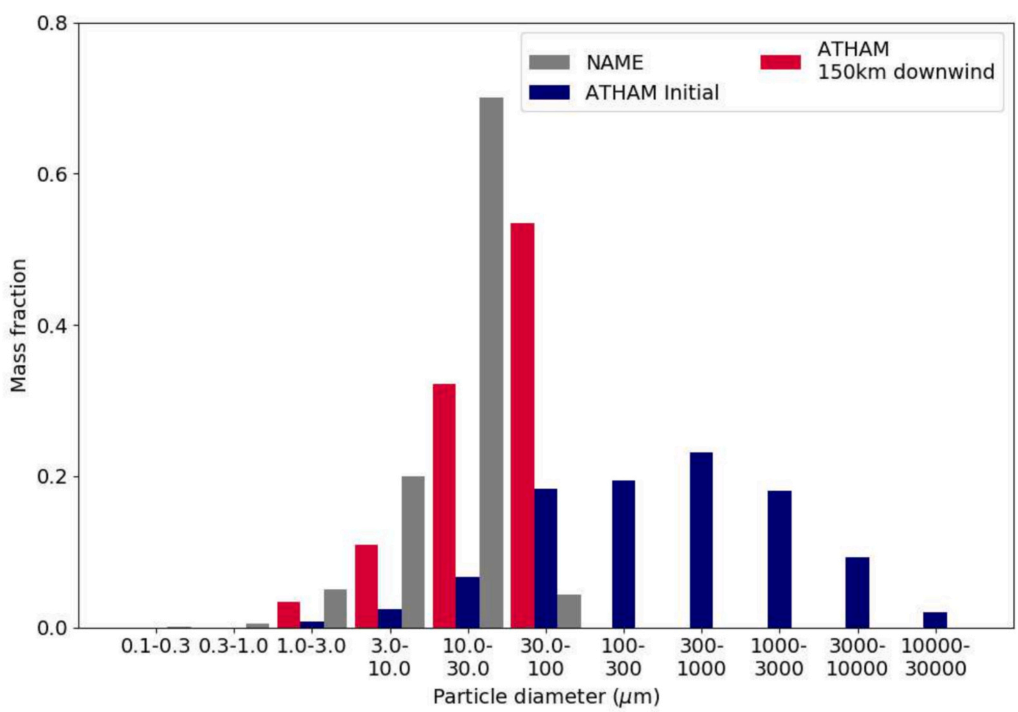

Fig. 5. Effective particle size distribution (PSD) used in NAME (grey), total PSD at the volcano vent in ATHAM (navy) and total PSD 150 km from the volcano vent in the ATHAM simulation (red). (For interpretation of the references to colour in this figure legend, the reader is referred to the web version of this article.)

negligible over this distance, although over a longer transport time it is also expected that the NAME effective PSD will evolve. The two particle diameter bins with the largest mass fractions have similar mass fraction magnitudes but the ATHAM total PSD is shifted to the right by one bin compared to NAME which has a peak assigned to the 10–30 μm bin and second highest mass fraction in the 3–10 μm bin. It is important to note that neither PSD shown here is designed to match the Raikoke 2019 eruption, plus aggregation is not included in this version of ATHAM so this might impact the particle size distribution away from the volcano vent. It should also be noted that ideally to complete a full comparison of the PSD the ATHAM simulation would need to be run for much longer to explore the behaviour in the distal plume. However, as discussed earlier, it is likely that particles > 100 μm diameter in the ATHAM simulation will not be transported 150 km downwind from the vent.

4. Discussion and conclusions

For the first time, the spatial distribution of ash and ash particle size distributions simulated using a 3D near-source plume rise model and an observationally constrained long-range dispersion model have been compared. The vertical profile of the effective mass eruption rate determined by the InTEM system is quasi uniform from 4 km to the maximum plume height (20 km and 16 km respectively for the ash and ash and clear sky iterations of InTEM). A comparison of the ash cloud 150 km downwind from the volcano vent shows that qualitatively the simulations produced using ATHAM and NAME-InTEM have a similar structure in both the horizontal and the vertical. After applying a scaling to the ATHAM simulation to ensure the time-integrated fine ash emission matches the time-integrated emission in the NAME-InTEM, the peak concentrations at 150 km have a similar vertical profile in both simulations. A comparison of the unscaled vertical profile of maximum ash concentration at 150 km shows higher concentrations of ash in the ATHAM simulations, which may be due to the choice of mass eruption rate chosen for the ATHAM simulations. The NAME-InTEM fine ash emissions indirectly account for near source loss process, such as particle aggregation, since they rely on the satellite detection of ash in the distal ash cloud. However, the ATHAM simulations do not currently account for aggregation processes. Therefore it is hypothesised that one reason for this difference is the missing representation of aggregation in ATHAM. Aggregation of particles can result in a significant reduction in the mass in the downwind ash cloud. For example, Rose et al. (2001) estimate from satellite observations of the 1992 eruptions of Crater Peak, USA, that the mass of fine ash (<25 mm diameter) was reduced by 90% due to hydrometeor-enhanced aggregation. The source inversion method results in a very similar distribution of ash to the computationally expensive 3D plume rise modelling method, for the assumed mass eruption rate used in ATHAM. Thus, we conclude that source inversion is a suitable alternative to constrain volcano vertical distribution of ash for real time operational forecasting. Although, we appreciate that there are existing methodologies that couple 1D plume rise models to dispersion models (e.g., Bruckert et al., 2021; Plu et al., 2021) which are computationally less expensive than a full 3D plume rise model such as ATHAM and are in semi-operational use (Icelandic Met Office, 2019). Ash concentrations in the ATHAM and NAME-InTEM simulations however differ by over an order of magnitude necessitating the application of a scaling to the ATHAM simulations in order to compare downwind ash distributions. Preset assumptions (Mastin et al., 2009 combined with a DFAF of 5 %) and source inversion methods result in ash concentrations both an order of magnitude larger and smaller than the near-source plume rise simulations respectively, suggesting that more research is needed to understand the sensitivity of long-range ash distribution to parameter choices made in the different methods. This range in ash concentration estimates could be due to missing processes (as described above), or too large a total mass eruption rate used in ATHAM, too large a fraction of mass contained in the fine ash particles which do not sediment out before reaching 150 km, or too small an estimate of the mass eruption by the InTEM source inversion. The use of a DFAF could also contribute to a discrepancy in between the two modelling system as there are many different estimates in the literature for this factor (e.g., Gouhier et al., 2019; Cashman and Rust, 2020) and it is likely to be time evolving and eruption specific. Assessing which of these is most likely to be the cause of the discrepancy should be the focus of future work.

As the plume rise model simulation progresses, the total PSD downwind from the volcano vent evolves to have a substantial peak in the 30–100 μm bin (almost 60% of the mass 150 km downwind). The total PSD at 150 km is much more similar to the preset effective PSD used in NAME than the total PSD that the ATHAM ash particles are initialised with, but with peaks in adjacent bins. This suggests that the assumption of near-source fall out of coarse ash particles in the representation of the preset effective particle size distribution used operationally in NAME holds fairly well.

The conclusions presented here are for one phase of a relatively short eruption of a stratospheric ash plume for one choice of ATHAM input parameters, including mass eruption rate and particle size distribution. Therefore further comparisons between ATHAM and NAME-InTEM for different types of eruptions should be performed to support the conclusions found here. It would also be informative to understand the impact of particle aggregation on the ATHAM estimates, especially in the case of phraetomagmatic eruptions (e.g. Eyjafjallajökull in 2010) which are impacted by the presence of large amounts of water at the volcano vent. Plus, there are studies that suggest that dry aggregation could also be as important as aggregation in the presence of water (e.g. Brown et al., 2012; Pollastri et al., 2021; Diaz-Vecino et al., 2023).

CRediT authorship contribution statement

Natalie J. Harvey: Conceptualization, Methodology, Software, Validation, Investigation, Resources, Writing – original draft, Writing – review & editing, Visualization. **Michael Herzog:** Resources, Writing – review & editing, Funding acquisition. **Helen F. Dacre:** Conceptualization, Methodology, Writing – original draft, Writing – review & editing, Funding acquisition. **Helen N. Webster:** Methodology, Software, Writing – review & editing.

Declaration of competing interest

The authors declare that they have no known competing financial interests or personal relationships that could have appeared to influence the work reported in this paper.

Acknowledgements

N.J.H. and H.F.D. are funded by the Natural Environment research council (NERC) grant number NE/S005218/1. M.H. is funded by NERC grant number NE/S004386/1. The authors would also like to thank M. Hort and D. Thomson at the Met Office for useful discussions about this work. We would also like to thank two anoymous reviewers for their fair and constructive comments that were used to improve the manuscript.

Data availability

The NAME, InTEM and ATHAM simulations run as part of this study are available in the University of Reading Research Data Archive at https://doi.org/10.17864/1947.001298. Further information about the data supporting these findings and requests for access to the data can be directed to. For InTEM and NAME licence enquiries, please contact the Met Office (atmospheric.dispersion@metoffice.gov.uk).

References

Arason, P., Petersen, G., Bjornsson, H., 2011. Observations of the altitude of the volcanic plume during the eruption of eyjafjallajökull, april-may 2010. Earth Syst. Sci. Data Discuss. 4, 1–25.

Aravena, A., Carparelli, G., Cioni, R., Prestifilippo, M., Scollo, S., 2023. Toward a real-time analysis of column height by visible cameras: an example from Mt. Etna, in Italy. Remote Sens. 15. https://doi.org/10.3390/rs15102595.

Aubry, T.J., Engwell, S., Bonadonna, C., Carazzo, G., Scollo, S., Van Eaton, A.R., Taylor, I.A., Jessop, D., Eychenne, J., Gouhier, M., Mastin, L.G., Wallace, K.L., Biass, S., Bursik, M., Grainger, R.G., Jellinek, A.M., Schmidt, A., 2021. The independent volcanic eruption source parameter archive (IVESPA, version 1.0): a new observational database to support explosive eruptive column model validation and development. J. Volcanol. Geotherm. Res. 417, 107295. https://doi.org/10.1016/j.jvolgeores.2021.107295.

Beckett, F.M., Witham, C.S., Hort, M.C., Stevenson, J.A., Bonadonna, C., Millington, S.C., 2015. Sensitivity of dispersion model forecasts of volcanic ash clouds to the physical characteristics of the particles. J. Geophys. Res. Atmos. 120, 11,636–11,652. https://doi.org/10.1002/2015JD023609.

Beckett, F.M., Witham, C.S., Leadbetter, S.J., Crocker, R., Webster, H.N., Hort, M.C., Jones, A.R., Devenish, B.J., Thomson, D.J., 2020. Atmospheric dispersion modelling at the London VAAC: a review of developments since the 2010 Eyjafjallajökull volcano ash cloud. Atmosphere 11, 352.

Bessho, K., Date, K., Hayashi, M., Ikeda, A., Imai, T., Inoue, H., Kumagai, Y., Miyakawa, T., Murata, H., Ohno, T., Okuyama, A., Oyama, R., Sasaki, Y., Shimazu, Y., Shimoji, K., Sumida, Y., Suzuki, M., Taniguchi, H., Tsuchiyama, H., Uesawa, D., Yokota, H., Yoshida, R., 2016. An introduction to himawari-8/9; japan's new-generation geostationary meteorological satellites. J. Meteorol. Soc. Jpn. Ser. II 94, 151–183. https://doi.org/10.2151/jmsj.2016-009.

Bonadonna, C., Folch, A., 2011. Ash Dispersal Forecast and Civil Aviation Workshop - Model Benchmark Document. URL: https://theghub.org/resources/505.
Bonadonna, C., Phillips, J.C., 2003. Sedimentation from strong volcanic plumes. J. Geophys. Res. Solid Earth 1978–2012, 108.
Brown, R., Bonadonna, C., Durant, A., 2012. A review of volcanic ash aggregation. Phys. Chem. Earth A/B/C 45-46, 65–78. https://doi.org/10.1016/j.pce.2011.11.001.
Bruckert, J., Hoshyaripour, G.A., Horváth, A., Muser, L., Prata, F.J., Hoose, C., Vogel, B., 2021. Online treatment of eruption dynamics improves the volcanic ash and SO_2 dispersion forecast: case of the Raikoke 2019 eruption. Atmos. Chem. Phys. Discuss. 2021, 1–23. https://doi.org/10.5194/acp-2021-459.
Bursik, M., 2001. Effect of wind on the rise height of volcanic plumes. Geophys. Res. Lett. 28, 3621–3624.
Cao, Z., Patra, A., Bursik, M., Pitman, E.B., Jones, M., 2018. Plume-SPH 1.0: a three-dimensional, dusty-gas volcanic plume model based on smoothed particle hydrodynamics. Geosci. Model Dev. 11, 2691–2715. https://doi.org/10.5194/gmd-11-2691-2018.
Cao, Z., Bursik, M., Yang, Q., Patra, A., 2021. Simulating the transport and dispersal of volcanic ash clouds with initial conditions created by a 3d plume model. Front. Earth Sci. 9. https://doi.org/10.3389/feart.2021.704797.
Capponi, A., Harvey, N.J., Dacre, H.F., Beven, K., Saint, C., Wells, C.A., James, M.R., 2021. Refining an ensemble of volcanic ash forecasts using satellite retrievals: Raikoke 2019. Atmos. Chem. Phys. Discuss. 2021, 1–28. https://doi.org/10.5194/acp-2021-858.
Carazzo, G., Jellinek, A., 2013. Particle sedimentation and diffusive convection in volcanic ash-clouds. J. Geophys. Res. Solid 118. https://doi.org/10.1002/jgrb.50155.
Cashman, K.V., Rust, A.C., 2020. Far-travelled ash in past and future eruptions: combining tephrochronology with volcanic studies. J. Quat. Sci. 35, 11–22. https://doi.org/10.1002/jqs.3159.
Cerminara, M., 2015. The Multiphase Buoyant Plume Solution of the Dusty Gas Model. arXiv preprint arXiv:1506.01638.
Cerminara, M., Ongaro, T.E., Neri, A., 2016. Large eddy simulation of gas–particle kinematic decoupling and turbulent entrainment in volcanic plumes. J. Volcanol. Geotherm. Res. 326, 143–171.
Costa, A., Suzuki, Y., Cerminara, M., Devenish, B., Ongaro, T.E., Herzog, M., Van Eaton, A., Denby, L., Bursik, M., de Michieli Vitturi, M., Engwell, S., Neri, A., Barsotti, S., Folch, A., Macedonio, G., Girault, F., Carazzo, G., Tait, S., Kaminski, E., Mastin, L., Woodhouse, M., Phillips, J., Hogg, A., Degruyter, W., Bonadonna, C., 2016. Results of the eruptive column model inter-comparison study. J. Volcanol. Geotherm. Res. 326, 2–25. https://doi.org/10.1016/j.jvolgeores.2016.01.017.
Crank, J., Nicolson, P., 1947. A practical method for numerical evaluation of solutions of partial differential equations of the heat-conduction type. In: Mathematical Proceedings of the Cambridge Philosophical Society. Cambridge University Press, pp. 50–67.
Dacre, H., Grant, A., Hogan, R., Belcher, S., Thomson, D., Devenish, B., Marenco, F., Hort, M., Haywood, J.M., Ansmann, A., et al., 2011. Evaluating the structure and magnitude of the ash plume during the initial phase of the 2010 Eyjafjallajökull eruption using lidar observations and name simulations. J. Geophys. Res. 116. https://doi.org/10.1029/2011JD015608.
Dacre, H., Grant, A., Johnson, B., 2013. Aircraft observations and model simulations of concentration and particle size distribution in the Eyjafjallajokull volcanic ash cloud. Atmos. Chem. Phys. 13, 1277–1291.
de Michieli Vitturi, M., Neri, A., Barsotti, S., 2015. Plume-mom 1.0: a new integral model of volcanic plumes based on the method of moments. Geosci. Model Dev. 8, 2447–2463. https://doi.org/10.5194/gmd-8-2447-2015.
Degruyter, W., Bonadonna, C., 2012. Improving on mass flow rate estimates of volcanic eruptions. Geophys. Res. Lett. 39. https://doi.org/10.1029/2012GL052566.
Denlinger, R.P., Pavolonis, M., Sieglaff, J., 2012. A robust method to forecast volcanic ash clouds. J. Geophys. Res. 117. https://doi.org/10.1029/2012JD017732.
Devenish, B., Thomson, D., Marenco, F., Leadbetter, S., Ricketts, H., Dacre, H., 2012. A study of the arrival over the United Kingdom in April 2010 of the Eyjafjallajökull ash cloud using ground-based lidar and numerical simulations. Atmos. Environ. 48, 152–164.
Diaz-Vecino, C., Rossi, E., Pollastri, S., Fries, A., Lemus, J., Bonadonna, C., 2023. Insights into the sticking probability of volcanic ash particles from laboratory experiments. Sci. Rep. 13, 21188.
Dioguardi, F., Beckett, F., Dürig, T., Stevenson, J.A., 2020. The impact of eruption source parameter uncertainties on ash dispersion forecasts during explosive volcanic eruptions. J. Geophys. Res. Atmos. 125. https://doi.org/10.1029/2020JD032717.
Dürig, T., Gudmundsson, M.T., Ágústsdóttir, T., Högnadóttir, T., Schmidt, L.S., 2022. The effect of wind and plume height reconstruction methods on the accuracy of simple plume models — a second look at the 2010 Eyjafjallajökull eruption. Bull. Volcanol. 84. https://doi.org/10.1007/s00445-022-01541-z.
Dürig, T., Gudmundsson, M.T., Dioguardi, F., Schmidt, L.S., 2023. Quantifying the effect of wind on volcanic plumes: implications for plume modeling. J. Geophys. Res. Atmos. 128. https://doi.org/10.1029/2022JD037781.
Folch, A., Costa, A., Macedonio, G., 2016. FPLUME-1.0: an integral volcanic plume model accounting for ash aggregation. Geosci. Model Dev. 9, 431–450. https://doi.org/10.5194/gmd-9-431-2016.
Francis, P.N., Cooke, M.C., Saunders, R.W., 2012. Retrieval of physical properties of volcanic ash using Meteosat: a case study from the 2010 Eyjafjallajökull eruption. J. Geophys. Res. 117. https://doi.org/10.1029/2011JD016788.
Girard, S., Korsakissok, I., Mallet, V., 2014. Screening sensitivity analysis of a radionuclides atmospheric dispersion model applied to the Fukushima disaster. Atmos. Environ. 95, 490–500.
Global Volcanism Program, 2019. Report on Raikoke (Russia). In: Crafford, A.E., Venzke, E. (Eds.), Bulletin of the Global Volcanism Network, 44. Smithsonian Institution, p. 8. https://doi.org/10.5479/si.GVP.BGVN201908-290250.
Gouhier, M., Eychenne, J., Azzaoui, N., Guillin, A., Deslandes, M., Poret, M., Costa, A., Husson, P., 2019. Low efficiency of large volcanic eruptions in transporting very fine ash into the atmosphere. Sci. Rep. 9, 1449.
Grainger, R.G., Peters, D.M., Thomas, G.E., Smith, A.J.A., Siddans, R., Carboni, E., Dudhia, A., 2013. Measuring volcanic plume and ash properties from space. In: Remote Sensing of Volcanoes and Volcanic Processes: Integrating Observation and Modelling. Geological Society of London. https://doi.org/10.1144/SP380.7.
Grant, A.L.M., Dacre, H.F., Thomson, D.J., Marenco, F., 2012. Horizontal and vertical structure of the Eyjafjallajökull ash cloud over the UK: a comparison of airborne lidar observations and simulations. Atmos. Chem. Phys. 12, 10145–10159.
Guerrieri, L., Corradini, S., Theys, N., Stelitano, D., Merucci, L., 2023. Volcanic clouds characterization of the 2020–2022 sequence of Mt. Etna lava fountains using msg-seviri and products' cross-comparison. Remote Sens. 15. https://doi.org/10.3390/rs15082055.
Harvey, N.J., Dacre, H.F., Webster, H.N., Taylor, I.A., Khanal, S., Grainger, R.G., Cooke, M.C., 2020. The impact of ensemble meteorology on inverse modeling estimates of volcano emissions and ash dispersion forecasts: Grímsvötn 2011. Atmosphere 11, 1022. https://doi.org/10.3390/atmos11101022.
Harvey, N.J., Dacre, H.F., Saint, C., Prata, A.T., Webster, H.N., Grainger, R.G., 2022. Quantifying the impact of meteorological uncertainty on emission estimates and the risk to aviation using source inversion for the Raikoke 2019 eruption. Atmos. Chem. Phys. 22, 8529–8545. https://doi.org/10.5194/acp-22-8529-2022.
Hersbach, H., Bell, B., Berrisford, P., Hirahara, S., Horányi, A., Muñoz-Sabater, J., Nicolas, J., Peubey, C., Radu, R., Schepers, D., Simmons, A., Soci, C., Abdalla, S., Abellan, X., Balsamo, G., Bechtold, P., Biavati, G., Bidlot, J., Bonavita, M., De Chiara, G., Dahlgren, P., Dee, D., Diamantakis, M., Dragani, R., Flemming, J., Forbes, R., Fuentes, M., Geer, A., Haimberger, L., Healy, S., Hogan, R.J., Hólm, E., Janisková, M., Keeley, S., Laloyaux, P., Lopez, P., Lupu, C., Radnoti, G., de Rosnay, P., Rozum, I., Vamborg, F., Villaume, S., Thépaut, J.N., 2020. The ERA5 global reanalysis. Q. J. R. Meteorol. Soc. 146, 1999–2049. https://doi.org/10.1002/qj.3803.
Herzog, M., Graf, H.F., Textor, C., Oberhuber, J.M., 1998. The effect of phase changes of water on the development of volcanic plumes. J. Volcanol. Geotherm. Res. 87, 55–74. https://doi.org/10.1016/S0377-0273(98)00100-0.
Herzog, M., Oberhuber, J.M., Graf, H.F., 2003. A prognostic turbulence scheme for the nonhydrostatic plume model ATHAM. J. Atmos. Sci. 60, 2783–2796. https://doi.org/10.1175/1520-0469(2003)060<2783:APTSFT>2.0.CO;2.
Horváth, A., Girina, O.A., Carr, J.L., Wu, D.L., Bril, A.A., Mazurov, A.A., Melnikov, D.V., Hoshyaripour, G.A., Buehler, S.A., 2021. Geometric estimation of volcanic eruption column height from GOES-R near-limb imagery – part 2: case studies. Atmos. Chem. Phys. 21, 12207–12226. https://doi.org/10.5194/acp-21-12207-2021.
Höskuldsson, Á., Janebo, M., Thordarson, T., Andrésdóttir, T.B., Jónsdóttir, I., Guðnason, J., Magnúsdóttir, A., 2018. Total Grain Size Distribution in Selected Icelandic Eruptions. Last accessed 3 December 2024.
Icelandic Met Office, 2019. Vespa - Volcanic Eruptive Source Parameter Assessment. http://brunnur.vedur.is/radar/vespa/. Accessed: 5 December 2024.
Jones, A., Thomson, D., Hort, M., Devenish, B., 2007. The UK Met Office's next-generation atmospheric dispersion model, NAME III. In: Air Pollution Modeling and its Application XVII. Springer, pp. 580–589.
Kristiansen, N.I., Stohl, A., Prata, A.J., Bukowiecki, N., Dacre, H., Eckhardt, S., Henne, S., Hort, M.C., Johnson, B.T., Marenco, F., Neininger, B., Reitebuch, O., Seibert, P., Thomson, D.J., Webster, H.N., Weinzierl, B., 2012. Performance assessment of a volcanic ash transport model mini-ensemble used for inverse modeling of the 2010 Eyjafjallajökull eruption. J. Geophys. Res. 117.
Lawson, C.L., Hanson, R.J., 1974. Solving Least Squares Problems. Prentice-Hall.
Lawson, C.L., Hanson, R.J., 1995. Solving least squares problems. In: Classics in Applied Mathematics. SIAM, Philadelphia.
Mastin, L.G., 2007. A user-friendly one-dimensional model for wet volcanic plumes. Geochem. Geophys. Geosyst. 8. https://doi.org/10.1029/2006GC001455.
Mastin, L., Guffanti, M., Servranckx, R., Webley, P., Barsotti, S., Dean, K., Durant, A., Ewert, J., Neri, A., Rose, W., Schneider, D., Siebert, L., Stunder, B., Swanson, G., Tupper, A., Volentik, A., Waythomas, C., 2009. A multidisciplinary effort to assign realistic source parameters to models of volcanic ash-cloud transport and dispersion during eruptions. J. Volcanol. Geotherm. Res. 186, 10–21.
Muser, L.O., Hoshyaripour, G.A., Bruckert, J., Horváth, A., Malinina, E., Wallis, S., Prata, F.J., Rozanov, A., von Savigny, C., Vogel, H., Vogel, B., 2020. Particle aging and aerosol–radiation interaction affect volcanic plume dispersion: evidence from the Raikoke 2019 eruption. Atmos. Chem. Phys. 20, 15015–15036. https://doi.org/10.5194/acp-20-15015-2020.
Neri, A., Esposti Ongaro, T., Macedonio, G., Gidaspow, D., 2003. Multiparticle simulation of collapsing volcanic columns and pyroclastic flow. J. Geophys. Res. Solid Earth 108.
Oberhuber, J.M., Herzog, M., Graf, H.F., Schwanke, K., 1998. Volcanic plume simulation on large scales. J. Volcanol. Geotherm. Res. 87, 29–53. https://doi.org/10.1016/S0377-0273(98)00099-7.
Oppenheimer, C., 1998. Review article: volcanological applications of meteorological satellites. Int. J. Remote Sens. 19, 2829–2864. https://doi.org/10.1080/014311698214307.
Osman, S., Beckett, F., Rust, A., Snee, E., 2020. Sensitivity of volcanic ash dispersion modelling to input grain size distribution based on hydromagmatic and magmatic deposits. Atmosphere 11. https://doi.org/10.3390/atmos11060567.

Pavolonis, M.J., Heidinger, A.K., Sieglaff, J., 2013. Automated retrievals of volcanic ash and dust cloud properties from upwelling infrared measurements. J. Geophys. Res. Atmos. 118, 1436–1458. https://doi.org/10.1002/jgrd.50173.

Pelley, R.E., Thomson, D.J., Webster, H.N., Cooke, M.C., Manning, A.J., Witham, C.S., Hort, M.C., 2021. A near-real-time method for estimating volcanic ash emissions using satellite retrievals. Atmosphere 12. https://doi.org/10.3390/atmos12121573.

Petersen, G.N., Bjornsson, H., Arason, P., von Löwis, S., 2012. Two weather radar time series of the altitude of the volcanic plume during the May 2011 eruption of Grímsvötn, Iceland. Earth Syst. Sci. Data 4, 121–127. https://doi.org/10.5194/essd-4-121-2012.

Plu, M., Bigeard, G., Sič, B., Emili, E., Bugliaro, L., El Amraoui, L., Guth, J., Josse, B., Mona, L., Piontek, D., 2021. Modelling the volcanic ash plume from Eyjafjallajökull eruption (May 2010) over europe: evaluation of the benefit of source term improvements and of the assimilation of aerosol measurements. Nat. Hazards Earth Syst. Sci. Discuss. 2021, 1–24. https://doi.org/10.5194/nhess-2021-97.

Pollastri, S., Rossi, E., Bonadonna, C., Merrison, J.P., 2021. Modelling the effect of electrification on volcanic ash aggregation. Front. Earth Sci. 8. https://doi.org/10.3389/feart.2020.574106.

Pouget, S., Bursik, M., Webley, P., Dehn, J., Pavolonis, M., 2013. Estimation of eruption source parameters from umbrella cloud or downwind plume growth rate. J. Volcanol. Geotherm. Res. 258, 100–112. https://doi.org/10.1016/j.jvolgeores.2013.04.002.

Prata, A.J., Prata, A.T., 2012. Eyjafjallajökull volcanic ash concentrations determined using spin enhanced visible and infrared imager measurements. J. Geophys. Res. Atmos. 117. https://doi.org/10.1029/2011JD016800.

Prata, A.T., Mingari, L., Folch, A., Macedonio, G., Costa, A., 2021. FALL3D-8.0: a computational model for atmospheric transport and deposition of particles, aerosols and radionuclides – part 2: model validation. Geosci. Model Dev. 14, 409–436. https://doi.org/10.5194/gmd-14-409-2021.

Prata, A.T., Grainger, R.G., Taylor, I.A., Povey, A.C., Proud, S.R., Poulsen, C.A., 2022. Uncertainty-bounded estimates of ash cloud properties using the ORAC algorithm: application to the 2019 Raikoke eruption. Atmos. Meas. Tech. 15, 5985–6010. https://doi.org/10.5194/amt-15-5985-2022.

Rose, W.I., Bluth, G.J., Schneider, D.J., Ernst, G.G., Riley, C.M., Henderson, L.J., McGimsey, R.G., 2001. Observations of volcanic clouds in their first few days of atmospheric residence: the 1992 eruptions of Crater Peak, Mount Spurr Volcano, Alaska. J. Geol. 109, 677–694.

Rossi, E., Bagheri, G., Beckett, F., Bonadonna, C., 2021. The fate of volcanic ash: premature or delayed sedimentation? Nat. Commun. 12, 1303.

Saint, C., Beckett, F.M., Dioguardi, F., Kristiansen, N., Tubbs, R.N., 2024. Using Simulated Radiances to Understand the Limitations of Satellite-Retrieved Volcanic Ash Data and the Implications for Volcanic Ash Cloud Forecasting. ESS Open Archive. https://doi.org/10.22541/au.171098669.97558978/v1.

Saxby, J., Beckett, F., Cashman, K., Rust, A., Tennant, E., 2018. The impact of particle shape on fall velocity: implications for volcanic ash dispersion modelling. J. Volcanol. Geotherm. Res. 362, 32–48. URL: https://www.sciencedirect.com/science/article/pii/S037702731830177X https://doi.org/10.1016/j.jvolgeores.2018.08.006.

Saxby, J., Rust, A., Cashman, K., Beckett, F., 2020. The importance of grain size and shape in controlling the dispersion of the vedde cryptotephra. J. Quat. Sci. 35, 175–185.

Schmehl, K.J., Haupt, S.E., Pavolonis, M.J., 2012. A genetic algorithm variational approach to data assimilation and application to volcanic emissions. Pure Appl. Geophys. 169, 519–537.

Smolarkiewicz, P.K., 1984. A fully multidimensional positive definite advection transport algorithm with small implicit diffusion. J. Comput. Phys. 54, 325–362. https://doi.org/10.1016/0021-9991(84)90121-9.

Sparks, R.S.J., Bursik, M., Carey, S., Gilbert, J., Glaze, L., Sigurdsson, H., Woods, A., 1997. Volcanic Plumes. Wiley.

Stohl, A., Prata, A., Eckhardt, S., Clarisse, L., Durant, A., Henne, S., Kristiansen, N., Minikin, A., Schumann, U., Seibert, P., et al., 2011. Determination of time-and height-resolved volcanic ash emissions and their use for quantitative ash dispersion modeling: the 2010 Eyjafjallajökull eruption. Atmos. Chem. Phys. 11, 4333–4351.

Suzuki, Y., Koyaguchi, T., 2009. A three-dimensional numerical simulation of spreading umbrella clouds. J. Geophys. Res. Solid Earth 114.

Suzuki, Y.J., Koyaguchi, T., Ogawa, M., Hachisu, I., 2005. A numerical study of turbulent mixing in eruption clouds using a three-dimensional fluid dynamics model. J. Geophys. Res. Solid Earth 110.

Suzuki, Y., Costa, A., Cerminara, M., Esposti Ongaro, T., Herzog, M., Van Eaton, A., Denby, L., 2016. Inter-comparison of three-dimensional models of volcanic plumes. J. Volcanol. Geotherm. Res. 326, 26–42. https://doi.org/10.1016/j.jvolgeores.2016.06.011.

Tadini, A., Roche, O., Samaniego, P., Guillin, A., Azzaoui, N., Gouhier, M., de Michieli Vitturi, M., Pardini, F., Eychenne, J., Bernard, B., Hidalgo, S., Le Pennec, J., 2020. Quantifying the uncertainty of a coupled plume and tephra dispersal model: PLUME-MOM/HYSPLIT simulations applied to Andean volcanoes. J. Geophys. Res. Solid Earth 125. https://doi.org/10.1029/2019JB018390.

Thomson, D.J., Webster, H.N., Cooke, M.C., 2017. Developments in the Met Office InTEM Volcanic Ash Source Estimation System Part 1: Concepts. URL: https://www.metoffice.gov.uk/research/library-and-archive/publications/science/weather-science-technical-reports.

Walters, D., Boutle, I., Brooks, M., Melvin, T., Stratton, R., Vosper, S., Wells, H., Williams, K., Wood, N., Allen, T., Bushell, A., Copsey, D., Earnshaw, P., Edwards, J., Gross, M., Hardiman, S., Harris, C., Heming, J., Klingaman, N., Levine, R., Manners, J., Martin, G., Milton, S., Mittermaier, M., Morcrette, C., Riddick, T., Roberts, M., Sanchez, C., Selwood, P., Stirling, A., Smith, C., Suri, D., Tennant, W., Vidale, P.L., Wilkinson, J., Willett, M., Woolnough, S., Xavier, P., 2017. The Met Office unified model global atmosphere 6.0/6.1 and JULES global land 6.0/6.1 configurations. Geosci. Model Dev. 10, 1487–1520. https://doi.org/10.5194/gmd-10-1487-2017.

Watson, E., Swindles, G., Stevenson, J., Savov, I., Lawson, I., 2016. The transport of Icelandic volcanic ash: insights from northern European cryptotephra records. J. Geophys. Res. Solid Earth 121, 7177–7192.

Webster, H., Thomson, D., 2011. Dry deposition modelling in a Lagrangian dispersion model. Int. J. Environ. Pollut. 47, 1–9.

Webster, H.N., Thomson, D.J., 2022. Using ensemble meteorological data sets to treat meteorological uncertainties in a Bayesian volcanic ash inverse modeling system: a case study, Grímsvötn 2011. J. Geophys. Res. Atmos. 127, e2022JD036469. https://doi.org/10.1029/2022JD036469.

Webster, H., Thomson, D., Johnson, B., Heard, I., Turnbull, K., Marenco, F., Kristiansen, N., Dorsey, J., Minikin, A., Weinzierl, B., et al., 2012. Operational prediction of ash concentrations in the distal volcanic cloud from the 2010 Eyjafjallajökull eruption. J. Geophys. Res. 117.

Webster, H.N., Thomson, D.J., Cooke, M.C., 2017. Developments in the Met Office InTEM Volcanic Ash Source Estimation System Part 2: Results. URL: https://www.metoffice.gov.uk/research/library-and-archive/publications/science/weather-science-technical-reports.

Webster, H.N., Whitehead, T., Thomson, D.J., 2018. Parameterizing unresolved mesoscale motions in atmospheric dispersion models. J. Appl. Meteorol. Climatol. 57, 645–657. https://doi.org/10.1175/JAMC-D-17-0075.1.

Woodhouse, M.J., Hogg, A.J., Phillips, J.C., Sparks, R.S.J., 2013. Interaction between volcanic plumes and wind during the 2010 Eyjafjallajökull eruption, Iceland. J. Geophys. Res. 118, 92–109. https://doi.org/10.1029/2012JB009592.

Woods, A.W., Kienle, J., 1994. The dynamics and thermodynamics of volcanic clouds: theory and observations from the April 15 and April 21, 1990 eruptions of Redoubt volcano, Alaska. J. Volcanol. Geotherm. Res. 62, 273–299. https://doi.org/10.1016/0377-0273(94)90037-X.

Zidikheri, M.J., Lucas, C., Potts, R.J., 2017a. Estimation of optimal dispersion model source parameters using satellite detections of volcanic ash. J. Geophys. Res. Atmos. 122, 8207–8232.

Zidikheri, M.J., Lucas, C., Potts, R.J., 2017b. Toward quantitative forecasts of volcanic ash dispersal: using satellite retrievals for optimal estimation of source terms. J. Geophys. Res. Atmos. 122, 8187–8206.